Desalination and Water Treatment
www.deswater.com
doi: 10.1080/19443994.2015.1119751

57 (2016) 21273–21285
September

Taylor & Francis
Taylor & Francis Group

Microstructure evolution and properties of YSZ hollow fiber microfiltration membranes prepared at different suspension solid content for water treatment

Xiaozhen Zhang[a,b,*], Shuaifeng Suo[a], Yuhua Jiang[a], Qibing Chang[a], Guozhao Ji[b], Xingqin Liu[c]

[a]*School of Material Science and Engineering & Key Laboratory of Inorganic Membranes, Jingdezhen Ceramic Institute, Jingdezhen 333403, P.R. China, Tel./Fax: +86 798 8499328; email: zhangxz05@126.com (X. Zhang), Tel. +86 798 8499678; email: 2431553358@qq.com (S. Suo), Tel./Fax: +86 798 8499678; emails: jiangyh8112@126.com (Y. Jiang), changqb1258@hotmail.com (Q. Chang)*

[b]*FIMLab—Films and Inorganic Membrane Laboratory, School of Chemical Engineering, The University of Queensland, Brisbane, Qld 4072, Australia, Tel. +61 7 3365 9740; email: g.ji@uq.edu.au (G. Ji)*

[c]*Department of Materials Science and Engineering, University of Science and Technology of China (USTC), Hefei, 230026, P.R. China, Tel. +86 551 3606249; email: xqliu@mail.ustc.edu.cn*

Received 14 May 2015; Accepted 3 November 2015

ABSTRACT

Yttria-stabilized zirconia (YSZ) hollow fiber ceramic membranes for microfiltration applications were prepared by the phase inversion and sintering technique. The influence of suspension solid content on the rheological behavior of suspension, and the microstructure and properties of the hollow fiber membranes were investigated. With the addition of YSZ powder, the viscosity of the spinning suspension increased obviously, and the rheological behavior of the suspension changed from Newtonian fluid into thinning behavior fluid. The increment of suspension viscosity upon the YSZ content led to a more porous inner surface, larger inner finger-like pores extending outward, and reduced outer finger-like layer for the prepared hollow fiber membrane. When the YSZ content was increased to 65%, a double-layer structure mostly consisting of outer sponge-like layer and inner finger-like structure layer was formed. The pure water flux of the hollow fiber membrane decreased with the increment of YSZ content, while the bending strength showed obvious enhancement. The prepared membranes showed good oil/water separation performance, and steady permeate flux of more than 0.85 $m^3/(m^2\ h\ bar)$ and high oil rejection rate of 99.2–99.7% were attained. Transmembrane resistance analysis indicated that the membranes prepared at 50 and 65% YSZ content had different dominant fouling mechanism in oil/water separation process.

Keywords: Hollow fiber ceramic membrane; Yttria-stabilized zirconia; Microfiltration; Microstructure evolution; Water flux; Oil/water separation

1. Introduction

Ceramic hollow fiber membranes fabricated by the phase inversion method have attracted considerable attention in the membrane community during the past 10 years [1–11]. Many special advantages offered by this type of membrane include large membrane area per unit volume (≥1,000 m^2/m^3) and excellent permeability due to the self-supporting asymmetrical

*Corresponding author.

1944-3994/1944-3986 © 2015 Balaban Desalination Publications. All rights reserved.

structure with thin separation layer [8,9]. Furthermore, with the employment of phase inversion method, the asymmetrical ceramic membranes can be fabricated in one step and with only once high-temperature sintering. Hence, the quality stability of the membrane can be improved, and the energy consumption and thus the cost of production is likely to be greatly reduced, compared to the traditional multi-layer ceramic membrane, whose preparation procedure involves multiple coating and sintering, and is time-consuming and costly [8,12]. Up to now, the ceramic hollow fiber membranes have gained extensive applications in many fields, including water treatment (e.g. oil/water separation and desalination) [13,14], gas separation [1–3], high temperature membrane reactors [15], solid oxide fuel cells [4,5], and membrane contactors [16] as well as supports for composite membranes [17] and catalysts [18].

Fabrication of ceramic hollow fiber membranes with both desirable morphology and separation performance for specific applications is still challenging. Many researches have verified that microstructure of the hollow fiber membranes plays a significant role in determining the membrane performance [3,8,14,19]. Actually, one of the unique advantages possessed by the phase inversion method lies in that the derived microstructure of the membranes is adjustable with good flexibility by choosing proper materials and by controlling the composition of suspension, related spinning parameters and sintering conditions. As shown by Liu et al., the YSZ hollow fiber membrane demonstrates a sandwich structure with the sponge-like layer in the middle and finger-like layer at the inner and outer sides when water is used as both the internal and external coagulants. This kind of structure is beneficial to increase the gas-tightness and bending strength of hollow fiber membranes after sintering at an enough temperature, and facilitates the YSZ membrane to be applied as the electrolyte of micro-SOFCs, oxygen separation membranes, etc. [10]. However, highly permeable asymmetrical porous YSZ hollow fiber membranes with excellent water permeability were attained when the composition of the internal/external coagulants is 90–100% NMP/water or water/ethanol in our previous work [8,14]. The air gap during spinning, particle size of ceramic powder and sintering temperature were also found to affect the microstructure and properties [11,20,21]. The composition of suspension composed of solid particle, polymer, solvent, and even non-solvent, is another significant factor to affect the membrane structure and performance in a more complex way, since it determines the initial thermodynamic and dynamic conditions for phase inversion and could influence the sintering process. It was found that varying the viscosity of the spinning suspension by adding water (non-solvent), the fiber morphology can be changed greatly [20]. However, few research involves the effects of solid content on the rheological behavior of suspension, and the microstructure, pore size distribution, porosity, water flux, and separation performance of hollow fiber membrane up to now. In this work, porous YSZ hollow fiber microfiltration (MF) membranes were prepared from suspensions with different solid content (at fixed polymer/solvent ratio). We investigated the influences of suspension solid content (YSZ content) on the viscosity and phase inversion process of suspensions and thus the microstructure and performance of derived hollow fiber MF membranes. The oil/water emulsion separation performance was also investigated for the resultant YSZ hollow fiber membranes with different microstructures. This would contribute to further fundamental understanding of phase inversion process of ceramic powder/polymer/solvent system, and is beneficial for optimizing the microstructure and performance of hollow fiber MF membranes for wastewater treatment.

2. Experimental

2.1. Materials

Yttria-stabilized zirconia (YSZ) powder was purchased from Jiujiang Fanmeiya Advanced Materials Co., Ltd. The YSZ powder has a narrow particle size distribution mainly in the range of 0.4–1.5 μm with a d_{50} = 0.8 μm. To prepare the polymer solutions, polyethersulfone (PES, ultrason E2010, from BASF chemical company, Germany) and N-methyl-2-pyrrolidinone (NMP, CP Grade, Sinopharm Chemical Reagent Co., Ltd, China) were used as the polymer binder and the solvent, respectively. Tap water was used as both the external and internal coagulants for the gelation of the extruded hollow fiber membrane precursors.

2.2. Preparation of YSZ hollow fiber membranes

The YSZ hollow fiber membranes were shaped by the immersion-induced phase inversion method based on a dry/wet spinning process, followed by heat-treatment at high temperature. The detailed preparation procedures were described elsewhere [8]. In this study, the spinning suspensions of polymer/solvent/ceramic powder system were prepared with different amount of YSZ powder (50, 55, 60, and 65% in mass fraction, the same below) and PES and NMP (the mass ratio of PES to NMP is fixed at 1:4). Tap water was

used as both the external and internal coagulants. The temperature of both coagulants is about 25℃, and the relative humidity of environment is 71%. The tube-in-orifice spinneret has an orifice diameter and inner diameter of 2.5 and 1.0 mm, respectively, and the degassed suspension was extruded through the spinneret at a nitrogen pressure of 0.3–0.7 bar. The injection rate of internal coagulant was kept at 30 ml/min. The fibers emerging from the spinneret at about 4.0 m/min passed through an air gap of 2 cm and were immersed in the water bath for complete solidification. The sintering process was conducted at the static air atmosphere. The dried YSZ hollow fiber membranes precursors were firstly heated up to 650℃ for 2 h at 2℃/min to remove the organic polymer binder and additive, and were then further increased to 1,350℃ for 4 h at 5℃/min.

2.3. Characterization

The particle size of YSZ powder was measured using laser particle size analyzer (Mastersizer 2000, Malvern instruments Ltd, UK). The rheological behavior (viscosity) of the PES/NMP/YSZ system suspensions was measured by the Bohlin V88 Viscometer (Malvern instruments Ltd, UK), with shear rate ranging from 0.1 to 400/s. The temperature was controlled by a heated and refrigerated Circulator, (F32, Julabo, Houston, USA). For comparison, the viscosity of 20% (mass fraction, the same below) PES solution in NMP without ceramic powder was also measured at the same conditions. Thermal behavior of the hollow fiber precursors from room temperature to 1,000℃ was examined by differential thermal analysis (DTA) and thermogravimetric (TG) measurement using a DTG-60H Thermal Analyzer (Shimadzu Scientific Instruments, Inc., Japan), with a heating rate of 10℃/min. Microstructure of the sintered hollow fiber membranes was observed with a scanning electron microscopy (SEM, model JSM-6390, JEOL, Japan) under the emission of secondary electrons. The pore size distribution (PSD) of the membranes was measured by a pore size analyzer (PSDA 20, Gaoqian Functional Materials Co., Ltd, China) based on the gas–liquid displacement technique, i.e. the so-called bubble point method. The samples were soaked in a mixture solution of organic solvents with low surface tension for 1 h under vacuum before the measurement. The porosity of hollow fiber membrane was measured by Archimedes method with pure water as the immersion liquid medium. The samples were cut into about 4 cm in length. To measure the quality of well-wetted samples more accurately, the outer surface was wiped with a wetted cotton cloth, followed by pulling a fine wetted cotton string, which was connected to a straight silver wire (diameter: 0.6 mm), through the lumen of the fiber in order to remove the water on both surfaces after the sample was taken out from the water. The pure water flux was measured in a dead-end permeation apparatus with applied transmembrane pressure in the range of 0.5–3.0 bar. Before the measurements of pure water permeate flux, all the samples were well wetted with the pure water. The mechanical strength was determined by a standard three point bending method using a universal testing machine (Instron 5566, Instron, America), with a crosshead speed of 0.50 mm/min and span length of 30 mm. The bending strength (σ_F) was calculated according to Eq. (1) [9]:

$$\sigma_F = \frac{8FLD}{\pi(D^4 - d^4)}) \quad (1)$$

where F is the measured force at which the fracture occurred and L, D, and d are the length (30 mm), the outside diameter (OD), and the inside diameter (ID) of the hollow fibers, respectively.

2.4. Filtration experiments

The prepared hollow fiber membranes were applied to separate the oil/water emulsion through the cross-flow filtration experiments conducted on a homemade filtration apparatus using an external pressure-type hollow fiber membrane module with 20 cm length fibers. The apparatus was run at a feed velocity of 3 m/s with a transmembrane pressure difference of 1.5 bar and a constant temperature of about 25℃. The constant feed concentration was maintained by recycling the filtrate back into the feed tank.

The oil/water emulsion used in this study was prepared by mixing mineral oil with pure water and surfactant (Tween-80 and Span-80) for 15 min using a blender (Fluko Equipment Shanghai Co., Ltd, China) at a different speeds (1,000–5,000 rpm), and the mass ratio of oil:Tween-80:Span-80 is 8:1:1. The oil concentration in water was 4 g/L. As shown in Fig. 1, the prepared stable oil/water emulsion has an average droplet size of 3.2 μm with more than 90% of the oil droplets being in the range of 1–10 μm as measured by a laser particle size analyzer (Mastersizer 2000, Malvern). The oil concentration was measured by an infrared photometric oil analyzer (ET1200, Euro, Shanghai, China). The well-known resistance-in-series (RIS) model that describes the membrane resistances was applied to investigate the fouling mechanism of the hollow fiber membranes. The RIS model can be expressed by Eq. (2) [22]:

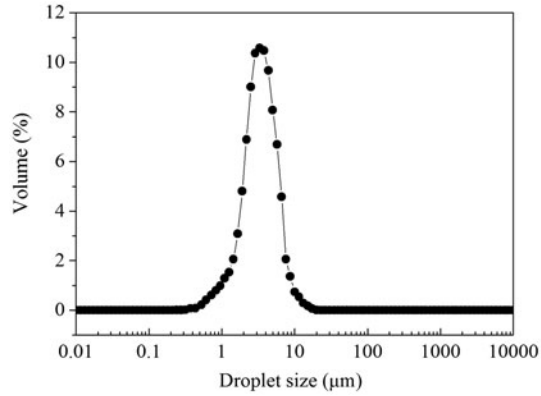

Fig. 1. Oil droplet size distribution of the feed emulsion.

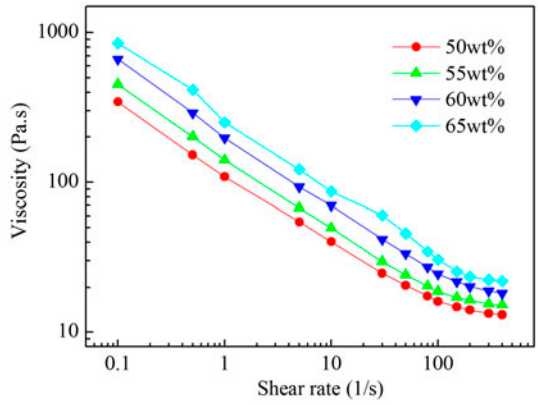

Fig. 2. Rheological behavior of the suspensions with different YSZ content.

$$J = \frac{\Delta P_m}{\mu(R_t)} = \frac{\Delta P_m}{\mu(R_m + R_{re} + R_{irr})} \quad (2)$$

where J is the permeate flux (m/s), ΔP is transmembrane pressure (Pa), μ is dynamic viscosity (Pa/s), R_t is total membrane resistance (1/m), R_m is new clean membrane hydraulic resistance (1/m), R_{irr} is irreversible resistance (due to adsorption, internal pore blockage, etc.) (1/m), and R_{re} is the reversible resistance (due to concentration polarization and/or cake layer formation) (1/m). The experimental procedure to determine each resistance value in the RIS model was described as following: (1) R_m was calculated by measuring the pure water flux at 25°C (without R_{irr} and R_{re}); (2) R_t was evaluated by the steady flux in the filtration of emulsion at 25°C; and (3) The membrane was then backflushed with pure water. The pure water flux was measured again at 25°C, to determine the resistance of $R_m + R_{irr}$. The irreversible resistance (R_{irr}) was calculated from steps (1) and (3) and the reversible resistance (R_{re}) from steps (2) and (3).

3. Results and discussion

3.1. Rheological property of suspensions

As for the hollow fiber membranes prepared by the immersion-induced phase inversion method, the rheological property of suspension (casting solution) is a very important factor influencing the membrane's properties and structure [23]. The PES/NMP system solution (20% PES) without YSZ powder showed an almost constant viscosity of about 0.75 Pa s with the shear rate ranging from 0.1 to 400/s, as is similar to the rheological behavior of Newtonian fluid. Fig. 2 shows the rheological behavior of PES/NMP/YSZ system suspensions with YSZ content in the range of 50–65%. As can be seen, the addition of YSZ powder greatly increases the viscosity and completely alters the rheological property of polymeric solution. The viscosity of all the suspensions with different YSZ contents decreases with the increment of shear rate, showing a typical shear thinning behavior (i.e. pseudoplastic flow behavior) [24]. The shear thinning behavior is caused by the destruction of gel structure (the interaction between particles) under applied shear stress. It can be found from Fig. 2 that higher YSZ content in suspension could lead to more obvious shear thinning behavior. But when the shear rate is increased up to more than 200/s, the change of the suspension viscosity becomes relatively small. Therefore, in the spinning process of suspensions with high solid content and thus high viscosity, it is necessary to appropriately increase the shear stress (i.e. increase the extrusion pressure) in order to reduce the viscosity and consequently obtain good fluidity of suspension.

3.2. Thermal analysis of hollow fiber precursor

Fig. 3 presents the DTA–TGA curves of dry YSZ hollow fiber precursor derived from the suspension having a solid content of 60%. The TGA curve indicates an obvious mass loss (about 10%) in the range of 500–600°C, and accordingly a very strong exothermic peak exists in the DTA curve, which could be attributed to the burnout of polymer PES. In addition, there is a weak exothermic peak in DTA curve at about 340°C, associated with a mass loss of 0.4%. This may be due to the volatilization of residual solvent NMP with low molecular weight, and indicates that most of the solvent NMP has been eliminated in the mass transfer process (exchange of solvent and non-solvent)

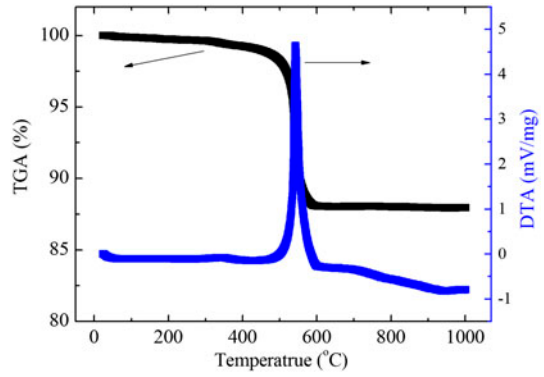

Fig. 3. TGA–DTA curves of the YSZ hollow fiber precursor.

when the nascent wet membrane was immersed into the coagulant of water. Based on the results of thermal analysis, a low heating rate of 2℃/min below 650℃ was chosen for the sintering of membrane, in order to avoid possible cracking and collapsing of the hollow fiber membrane.

3.3. Microstructure of the hollow fiber membranes

Fig. 4 shows the cross-sectional SEM images of the YSZ hollow fiber membranes derived from the suspensions with different YSZ content and sintered at 1,350℃ for 4 h. It can be seen from Fig. 4(a)–(d) that the OD and ID of the prepared hollow fiber are about 1.5 and 1.2 mm, respectively. The micrograph of Fig. 4(A) illustrates that with the YSZ content of 50%, the prepared hollow fiber membrane possesses a typical sandwich structure, i.e. a sponge-like layer in the center and short finger-like structure at the inner and outer sides. This appearance of the membrane microstructure can be attributed to rapid precipitation occurring at both sides resulting in finger-like structure, and slow precipitation giving the sponge-like structure in the middle of the fiber cross-section [10]. Nevertheless, the inner finger-like structure layer shows larger pore size than the outer counterpart, though they have similar thickness. This may be due to the existence of a 2-cm air gap, where simultaneous moisture absorption and solvent evaporation cause a local viscosity increase in the outer region of the fiber prior to immersion, and to some extent inhibit the growth of the outside finger-like structure [20]. It can be observed from Fig. 4(A), in combination with Fig. 5(a) and (A), very thin skin layers are also formed at both sides, and the produced finger-like pores do not penetrate through to the inner and outer surfaces. In the spinning process, once the nascent wet membrane precursor was in contact with the external and internal coagulants (water), rapid exchange of the solvent NMP, and water occurred near the surfaces, resulting in a sudden increase in the surface polymer concentration and consequently the polymer solidified to form the thin skin layers. According to the phase inversion mechanism, it is generally believed, that the formation of the inner and outer skin layers follows the spinodal decomposition mechanism, while the formation of the finger-like structure can be ascribed to the nucleation and growth of the polymer lean phase, i.e. the nuclei of the polymer lean phase grow up to form the finger-like pores [25–27]. The exchange of solvent and coagulant becomes difficult in the middle of fiber cross-section, and thus the growth of the

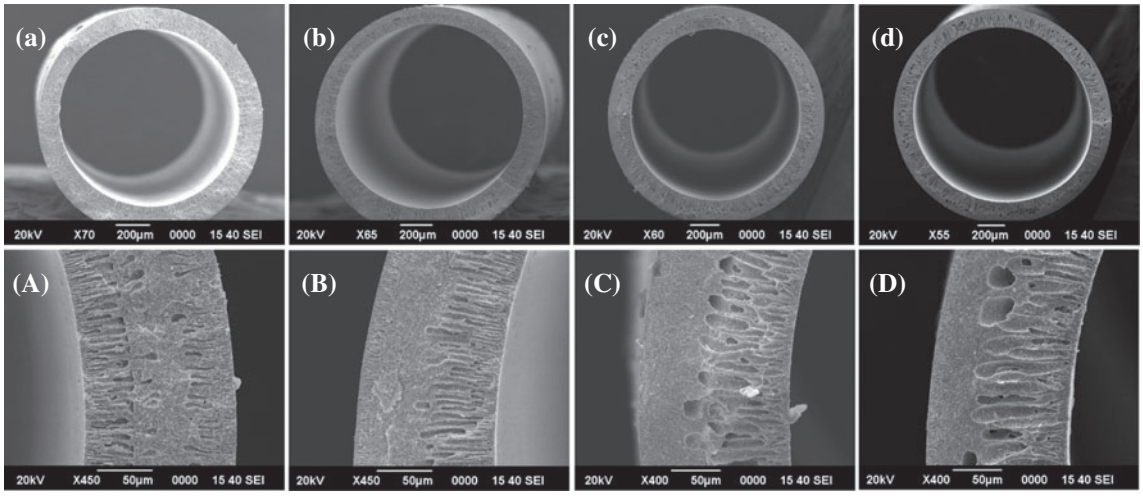

Fig. 4. Cross-sectional SEM images of the YSZ hollow fiber membrane prepared with suspensions of different YSZ content (1,350℃/4 h): (a–d) overall view, (A–D) cross section; (a and A) 50%, (b and B) 55%, (c and C) 60%, (d and D) 65%.

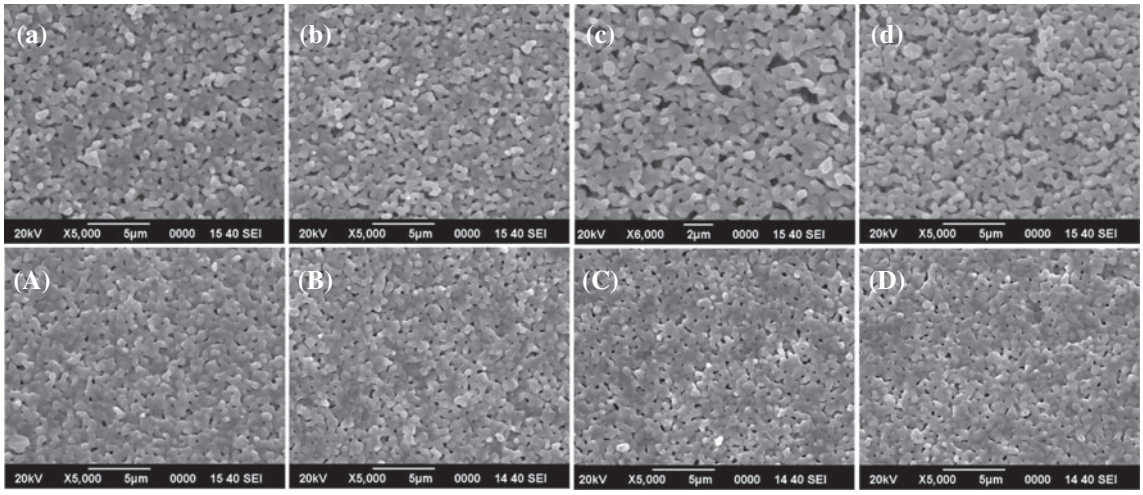

Fig. 5. Surface SEM images of the YSZ hollow fiber membrane prepared with suspensions of different YSZ content (1,350˚C/4 h): (a–d) inner surface, (A–D) outer surface; (a and A) 50%, (b and B) 55%, (c and C) 60%, (d and D) 65%.

nuclei is hindered resulting in the formation of the sponge-like structure layer [25]. When the YSZ content is increased to 55%, as can be found in Fig. 4(B), the inner finger-like structure layer enlarges toward the outside to occupy about 50% of the fiber cross-section, while the outer finger-like structure layer diminishes to be about 15% of the fiber cross-section with much smaller and shorter finger-like pores.

Fig. 4(C) and (D) demonstrate that when the solid content of the suspension is further increased to 60 and 65%, the outer finger-like structure almost disappears, and mostly a two-layer structure is formed with inner large finger-like structure layer and outer sponge-like layer. Furthermore, the relative thickness and pore size of the inner finger-like layer are enhanced obviously with the increment of YSZ content. The SEM analysis clearly manifests that the solid content (YSZ content) has significant effect on the microstructure of the resultant hollow fiber membranes. According to the phase inversion mechanisms, the phase inversion process for membrane formation is determined by the thermodynamic and dynamic conditions, as well as the interactions between the components. In this research, the PES/NMP ratio of the suspensions and the spinning parameters were kept unchanged, and the thermodynamic conditions in theory is mainly dependent on the composition of polymer solution. Hence, the microstructure evolution shown in Fig. 4 mostly results from the variation of dynamic condition of phase inversion. Actually, the greatly increased viscosity (shown in Fig. 2) resulted from the addition of YSZ powder has changed the dynamic condition of phase inversion. The above-described microstructure evolution upon the increase in YSZ content can be interpreted in terms of the suspension viscosity as well as the applied spinning parameters (mainly relative humidity and air gap). On the one hand, for the outside surface region, the increment of YSZ content from 50 to 55% obviously increases the local viscosity. In addition, with the existence of air gap, moisture absorption, and some water diffusion from the inner side prior to immersion further increase the viscosity of the outer region. Once the wet membrane precursor is immersed into the external coagulant, the high viscosity of the outer region inhibits the phase inversion process, and at the same time leads to slow nucleation and growth, for which only short and small finger-like pores are formed in the outer side. When the YSZ content is increased to 60 and 65%, the viscosity of the outer region of wet membrane prior to immersion has reached or even exceeded the upper critical value for rapid precipitation to take place. As a result, slow precipitation occurs to produce the sponge-like structure layer. On the other hand, for the inner region of the nascent membrane, the increase in suspension viscosity would also reduce the phase inversion rate to some extent (but the phase inversion process is still rapid precipitation), and the solidifying rate of the inner region decreases accordingly. Under this circumstance, more water can penetrate towards outside by means of mass transfer and exchange, facilitating the phase inversion to advance outward, and large finger-like structure takes shape since the advantage of nucleation and growth is not restrained. Therefore, it can be anticipated that a symmetrical structure will be formed for the hollow fiber membrane if the viscosity of the suspension is increased up to a critical point at

a certain higher YSZ content, where the phase inversion at both sides would be greatly retarded because of very low mass transfer rate between solvent (NMP) and coagulant (water). Similar phenomenon was observed by Kingsbury and Li in the preparation of Al_2O_3 hollow fiber membranes [20]. When non-solvent of water was added into the suspension, the increase in suspension viscosity led to the inhibited phase separation, and symmetric Al_2O_3 hollow fiber membrane was obtained with the addition of 10% water.

Fig. 5 shows the inner and outer surface SEM images of the YSZ hollow fiber membranes prepared at different YSZ content of suspension and sintered at 1,350℃ for 4 h. As illustrated in the figures, the inner surface shows a much more porous structure than the outer surface at the same YSZ content, and the pore size and roughness of the inner surface increase with the increment of YSZ content. This can be explained as follows: (1) the flow of internal coagulant, which imposes a shear stress to the inner surface of the nascent wet membrane, brings the YSZ particles which are still not immobilized by the polymer to move, and makes the inner surface unable to form a relatively dense skin layer as the outer surface; (2) the increase in suspension viscosity at higher YSZ content reduces the mass exchange rate of internal coagulant (water) and solvent (NMP) near the inner surface, and thus the solidifying rate of the inner surface. In this case, small YSZ particles on the inner surface are more likely to be driven to move by the internal flow. This eventually results in a rougher and more porous inner surface as shown in Fig. 5(a)–(d). The micrographs of Fig. 5(A)–(D) illustrate that the prepared hollow fiber membranes possess a homogeneous and smooth outer surface with well-distributed small pores. With a close observation, it can also be found that the outer surface porosity increases gradually with the increment of YSZ content from 50 to 60%, but shows no obvious change with further increment from 60 to 65%. This can also be attributed to the depressed precipitation dynamic condition resulting from the increased viscosity of suspension at higher YSZ content [23]. Higher rapid precipitation rate is more favorable to form the dense skin layer. The microstructure observation also indicates that in actual liquid filtration applications, the prepared hollow fiber membranes are suitable to be used in the external-pressure operation mode with outer skin layer as the separation layer [8].

It is worth noting that the solid content of suspensions also has significant effect on the flexibility of the solidified hollow fiber membrane precursors. For the suspension with a YSZ content of 50 and 65%, dried hollow fiber membrane after phase inversion has a corresponding YSZ content of about 83.3 and 90.3%, respectively (assuming that no NMP remained in the membranes after phase inversion). More YSZ solid particles are incorporated into the hollow fiber membrane at higher YSZ content, and the dried membrane would become more brittle. Our experiments show the YSZ content should be no more than 65% at a NMP/PES ratio of 4, otherwise the dried hollow fiber membrane is easy to fracture in the following fabrication process because of the increased brittleness.

3.4. Porosity and PSD

Fig. 6 presents the porosity of the YSZ hollow fiber membranes prepared at different YSZ content and sintered at 1,350℃ for 4 h. As can be seen, the porosity of the membranes obviously decreases with the YSZ content, and the hollow fiber membrane derived from the suspension with 65% YSZ shows the smallest porosity of 42.7%. This seems conflicting with the morphology observations in Fig. 4(A)–(D), where the finger-like pores become larger and the inner surface gets more porous with the increase in YSZ content in the suspension. It can be found from Fig. 7 that the particle packing density of the sponge-like layer and the finger-like pore wall of the prepared hollow fiber membranes increase significantly with the increment of YSZ content from 50 to 65%. So, the decrease in membrane porosity may be ascribed to the much denser sponge-like layer and finger-like pore wall. But despite this, the overall porosity (47.8–42.7%) of the prepared hollow fiber membranes is much higher than the common planar and tubular ceramic MF membrane (about 35%). This can be contributed to the highly asymmetrical structure with the porous inner

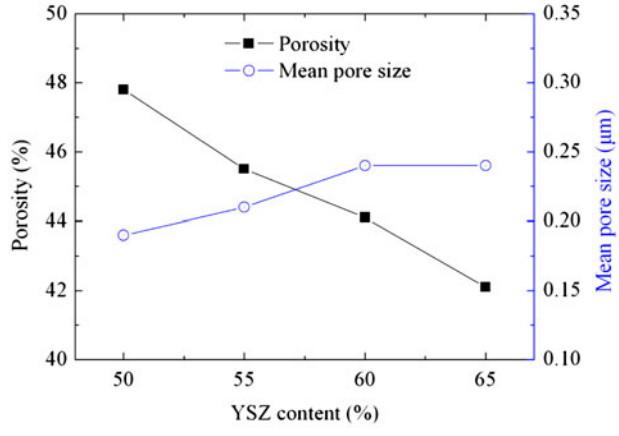

Fig. 6. Porosity and MPS of the YSZ hollow fiber membranes as a function of YSZ content in the suspensions.

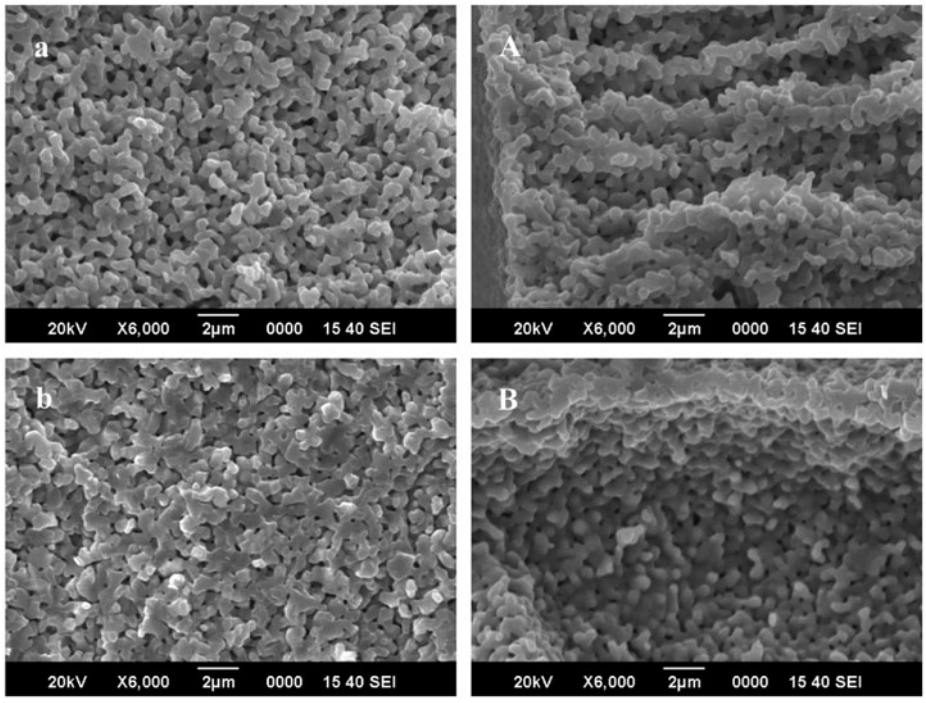

Fig. 7. Sponge-like layer (a and b) and finger-like pore (A and B) SEM images of the hollow fiber membranes with (a and A) 50% and (b and B) 65% YSZ content and sintered at 1,350℃ for 4 h.

surface and large finger-like pores. Generally, higher porosity is beneficial to decrease the transmembrane resistance and increase the water permeability of hollow fiber membranes for water treatment applications.

Fig. 6 also shows the mean pore size (MPS) of the prepared hollow fiber MF membranes. In this study, the PSD and MPS of hollow fiber membranes are measured by means of the bubble point method. So, it is reasonable to consider that the measured results mainly represent the pore size of the outer skin layer, based on microstructure analyses shown in Figs. 4, 5, and 7. As can be seen in Fig. 6, the variation of MPS with YSZ content is minor compared to porosity. The hollow fiber membrane prepared with the suspension solid content of 50% has a MPS of 0.19 μm, and a small increase in MPS is observed with solid content increasing to 60%, where a maximal MPS of 0.24 μm is obtained. Hereafter, no obvious change occurs with further increment of YSZ content to 65%. The change of MPS agrees well with the observation of Fig. 4(A)–(D). Fig. 8 shows the corresponding PSDs of the YSZ hollow fiber membranes prepared at different solid content of the suspension. As can be seen, the hollow fiber membrane prepared with 50% YSZ in the suspension shows the narrowest PSD. With the increment of YSZ content, the PSD of the membrane becomes wider, especially when the YSZ content reaches up to

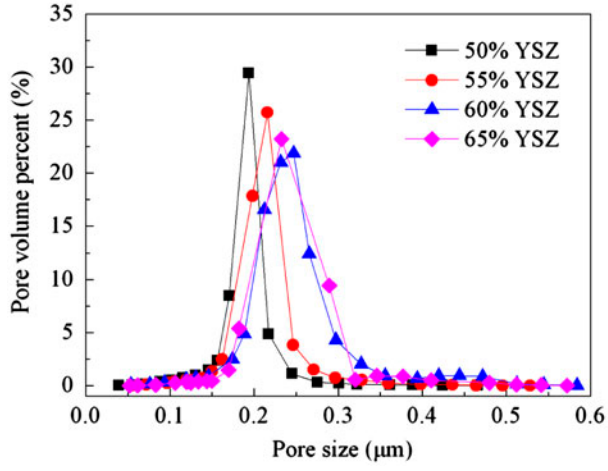

Fig. 8. PSDs of the YSZ hollow fiber membranes prepared at different suspension solid content.

60%. But on the whole, the PSDs of the prepared hollow fiber membranes are much narrower than that of ceramic membrane which is prepared by dip-coating technique on support and has similar MPS. For the latter, the largest pore size is often 3–5 times of the MPS [12]. In a word, the achieved narrow PSD and homogeneous morphology of the prepared hollow fiber membranes should be attributed to the

advantages of phase inversion method, as well as the narrow particle size distribution of the used YSZ powder. The prepared hollow fiber membranes with narrow PSD would have good potential for some fine microfiltration applications, e.g. water treatment, juice clarification, beer sterilization, drug separation, and purification.

3.5. Pure water flux and bending strength

Pure water flux can be used to evaluate the transmembrane resistance. The influence of YSZ content on the pure water flux of the prepared YSZ hollow fiber membranes is illustrated in Fig. 9. As can be seen, the pure water flux decreases with the increment of YSZ content in the suspension, being 3.07 and 2.13 $m^3/(m^2\ h\ bar)$ at the YSZ content of 50 and 65%, respectively. Li et al. presented a model to describe the relationship between pure water flux and structural parameters of sintered ceramic membranes [28]. The model can be expressed in the form of the modified Carman–Kozeny equation (Eq. (3)) and applied in Darcy's Law.

$$J = \frac{d_m^{k_2}\varepsilon^3\Delta P}{k_1\mu L(1-\varepsilon)^2} \tag{3}$$

where J is the pure water flux, ΔP is the transmembrane pressure difference, ε is the porosity, d_m is the MPS, L is the membrane thickness, and μ is the pure water viscosity, k_1 and k_2 are the constant developed by experimental data as correction factors for the deformation of ceramic particles and change in particle aggregation. Fung et al. verified that the modified equation can be applied to estimate the MPS of active layer (separation layer) of ceramic hollow fiber membranes with good fitness using the measured values of pure water flux and porosity [19]. Eq. (3) indicates that high porosity and large MPS are desirable to achieve higher pure water flux and thus lower permeate resistance of membranes. Hence, the obvious decrease in pure water flux with the increment of YSZ content in Fig. 9 may be mostly ascribed to the reduction of porosity, though the MPS shows a minor increment. Based on the foregoing microstructure analysis, it can be concluded that the permeate resistance of the prepared hollow fiber membranes are mostly derived from relative dense outer skin layer and sponge-like structure layer. As can be observed in Fig. 7, the compactness of sponge-like layer obviously increases with the increment of YSZ content. As a consequence, although the increment of solid content could increase the size of inner finger-like pores and lead to more porous inner surface, contributing to lower permeate resistance to some extent, the decrease in porosity of sponge-like layer and finger-like pore wall has become the dominant factor resulting in the decrease in pure water flux. Actually, in our previous study, it is found that thin thickness or the elimination of sponge-like layer could lead to greatly increased water permeability and thus much lower permeation resistance of hollow fiber membranes [8].

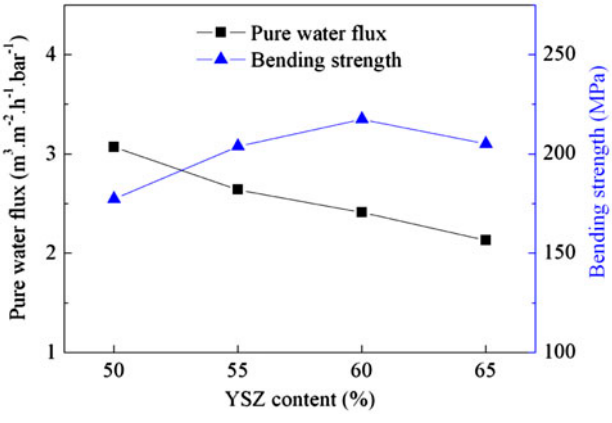

Fig. 9. Pure water flux and bending strength of the YSZ hollow fiber membranes as a function of YSZ content in the suspension.

For porous ceramic materials with certain composition, their porosity or density, pore size, and shape have significant effect on the mechancial strength. On the one hand, the reduction in porosity (increase in density) is beneficial to raise the mechanical stength, on the other hand, even few large pores would be fatal to the strength. Fig. 9 shows the bending strength of the prepared YSZ hollow fiber membranes. As can be seen, the increase in YSZ content leads to the enhancement of bending strength, until the YSZ content of 60% is reached and the bending strength starts to decrease when the YSZ content is further raised. The lowest bending strength is 177.3 MPa at a YSZ content of 50%, while the highest value of 217.5 MPa is attained when the YSZ content is raised to 60%. The influence of YSZ content on the bending strength can be explained by the above-described change of microstructure and porosity of the hollow fiber membranes. As can be observed in Fig. 7(a), for the membrane prepared at the YSZ content of 50% and sintered at 1,350°C for 4 h, the YSZ particles are loosely connected, leading to high porosity (47.8%) and bad bonding strength between most of the particles, and accordingly the mechanical strength of the hollow fiber membranes is low. When the YSZ content

was raised to 60%, the membrane should have much higher original packing density of particles, which promotes the sintering and densification of membranes at the same sintering conditions. Actually, by comparing Fig. 7(a) and (b), it is found that much better neck-bonding between particles is achieved in this case. Furthermore, the porosity decreases to 44.1%. All these contribute to the enhancement of bending strength with the increment of YSZ content from 50 to 60%. However, the bending strength decreases to 205.1 MPa with further increment of YSZ content to 65%, even though the membrane has the lowest porosity. This may be due to the existence of more large finger-like pores, which causes significant adverse effect to the mechanical strength.

3.6. Oil/water emulsion separation properties

The hollow fiber membranes of two different asymmetrical microstructures, which were prepared at 50 and 65% YSZ content, respectively, were applied to separate the oil/water emulsion. The oil/water emulsion separation properties were measured after running for 5 min and with a transmembrane pressure of 1.5 bar. Fig. 10 illustrates the permeate flux and oil rejection rate of the two hollow fiber membranes with a run-time of 3 h. As can be seen, for each hollow fiber membrane, its flux in oil/water separation is much lower than the pure water flux shown in Fig. 9, and the permeate flux decreases significantly during the initial 20–25 min for the two membranes. This is caused by the well-known concentration polarization, cake layer formation, internal adsorption, and/or pore plugging [29]. The pure water flux of the membrane prepared with 50% YSZ content is 44.1% higher than

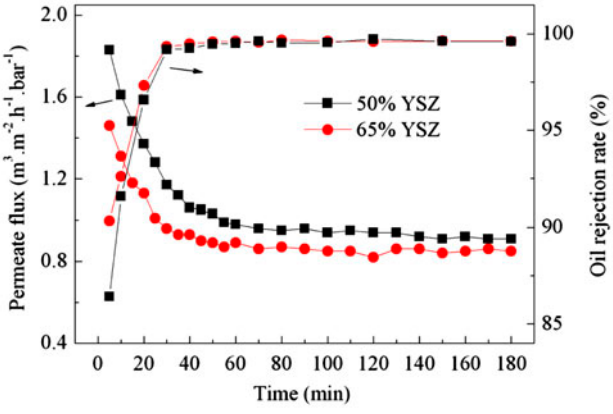

Fig. 10. Permeate flux and oil rejection rate in oil/water separation of the YSZ hollow fiber membranes prepared at the YSZ content of 50 and 65%.

that of the membrane prepared with 65% YSZ content in the suspension. Nevertheless, the difference in permeate flux decreases obviously with run-time in the oil/water separation process as shown in Fig. 10. After running for 3 h, the membranes show similar steady flux, being 0.91 and 0.85 $m^3/(m^2\,h\,bar)$ at the YSZ content of 50 and 65%, respectively. This indicates that the membrane fouling resulting from the emulsion has increased the permeate resistance of the two membranes at different levels, as could be ascribed to their different microstructure characteristics. Hence, in order to clarify the fouling mechanism of membranes with different microstructure, the well-known resistance-in-series (RIS) model was applied to investigate individual resistances of the two membranes during the separation process. The contribution of each kind of resistance was evaluated separately, and the results were summarized in Table 1. It is found that the hollow fiber membrane prepared at 50% YSZ content shows much higher fouling resistance (the sum of R_{irr} and R_{re}) than that prepared at 65% YSZ content, though the former shows much lower intrinsic hydraulic resistance (R_m). The reversible fouling resistance (R_{re}) due to cake formation is dominant in determining the overall filtration resistance for the membrane prepared at 50% YSZ content, while both the intrinsic hydraulic resistance and reversible resistance play a significant role for the membrane prepared at 65% YSZ content. The irreversible fouling resistance (R_{irr}) derived from the surfactant and oil adsorption and/or pore plugging by oil droplets is also the main cause of membrane fouling. As shown in Table 1, for the membrane prepared at 50% YSZ content, the R_{irr} accounts for 17.4% of the total resistance. However, the ratio of R_{irr}/R_t decreases to only 10.5% when the YSZ content was increased to 65%. The fouling resistance analysis indicates that the hollow fiber membrane prepared with suspension of 65% YSZ would be favorable to decrease the overall fouling resistance. Since both membranes have similar pore size which is much smaller than the oil droplet size, the larger fouling resistance of the former maybe due to the much higher initial water flux. Higher water flux drives more oil droplets to deposit on the membrane surface to form the cake layer quickly, and some small droplets are more likely to deform and dragged into the pores, resulting in more serious surface fouling, internal adsorption, and even plugging. According to the flux attenuation tendency with run-time shown in Fig. 10, it can be inferred that the hollow fiber membrane prepared at 50% YSZ content would lose its advantage in the long-term permeate flux to the hollow fiber membrane prepared at 65% YSZ content at the same filtration operation condi-

Table 1
Fouling resistances of the hollow fiber membranes prepared at 50 and 60% YSZ content of suspension after run for 3 h

Fouling resistances	Membrane at 50% YSZ	Membrane at 65% YSZ
R_t (10^{11}/m)	3.63	3.89
R_m (10^{11}/m)	1.31	1.89
R_{irr} (10^{11}/m)	0.63	0.41
R_{re} (10^{11}/m)	1.69	1.59
R_m/R_t (%)	36.1	48.6
R_{irr}/R_t (%)	17.4	10.5
R_r/R_t (%)	46.5	40.9

tions. Therefore, it can be concluded that the hollow fiber membrane with higher pure water flux does not necessarily possess high permeate flux in the filtration of oily water. But the improvement of oil/water separation performance for the membrane prepared at 50% YSZ content is possible by further optimization of related operation conditions according to the membrane characteristics, such as transmembrane pressure, feed cross-flow velocity, and cleaning process. Overall, the permeate flux values of the prepared YSZ hollow fiber membranes are much higher than those of the common tubular ceramic MF membranes with close pore size, which are usually less than 0.5 $m^3/(m^2$ h bar) [29–31]. For the latter, the percentage of irreversible resistance which is difficult to be eliminated, is often more than 30%.

It can be seen from Fig. 10 that the oil rejection rate increases sharply for both membranes in the initial 20 min and then reaches high values in the range of 99.2–99.7%. In the initial stage, the membrane prepared at 50% YSZ content shows a little lower rejection rate than that prepared at 65% YSZ content. This is maybe because stable cake layer is still not formed at this time and more small oil droplets can penetrate through the membrane in the case of much higher flux. Overall, the difference in oil rejection rate of both membranes is minor in this study. According to the obtained filtration results, it can be concluded that the prepared YSZ hollow fiber membranes have excellent performance in the microfiltration separation of oil/water emulsion. This must be ascribed to the asymmetrical structure with high porosity and thin wall thickness to decrease the intrinsic permeate resistance, as well as narrow PSD to reduce internal fouling and increase oil rejection. Therefore, the prepared hollow fiber membranes would have a good prospect in the treatment of industrial oily wastewater. But the optimization of operation parameters, such as transmembrane pressure, feed cross-flow velocity, oil concentration of feed and oil droplet size, is still needed according to the nature of oily water in practical applications.

4. Conclusions

Porous YSZ hollow fiber ceramic membranes for microfiltration can be fabricated with 50–65% YSZ solid content of suspension by the combination of phase inversion method and sintering at 1,350℃ for 4 h. The addition of ceramic powder altered the rheological behavior of suspension changing from the Newtonian fluid into the thinning behavior fluid, and the viscosity of the suspension increased greatly with the increment of YSZ content. The microstructure and properties of porous YSZ hollow fiber membranes can be tailored by changing the YSZ content and thus the viscosity of the suspension. Relative low viscosity at the YSZ content of 50% led to a typical sandwich structure mostly composed of finger-like structure at both sides and sponge-like layer in the middle. The increment of suspension viscosity due to increasing solid content resulted in larger inner finger-like pores extending outward, reduced outer finger-like layer, and more porous inner surface. The hollow fiber membrane derived from the suspension with 65% YSZ had the highest viscosity, and showed a double-layer structure mostly consisting of outer sponge-like layer and inner large finger-like structure. The porosity of the membranes decreased with the increment of YSZ content, while the MPS showed a minor increase from 0.19 to 0.24 μm and the PSD became wider. The increment of YSZ content also led to obvious reduction of pure water flux and the enhancement of bending strength. In the separation of oil/water emulsion, the hollow fiber membranes prepared at 50% YSZ content showed much higher initial permeate flux, but also faster decay than that prepared at 65% YSZ content. This resulted in close steady permeate flux for the two membranes after run 3 h. The oil rejection rate enhanced sharply during the initial stage and a high rejection rate of 99.2–99.7% was attained after run for 20–30 min for both membranes. Transmembrane resistance analysis according to the RIS model showed that the reversible fouling resistance due to

cake formation was dominant in determining the total resistance for the membrane prepared with 50% YSZ content, while both the intrinsic hydraulic resistance and reversible resistance played a significant role for the membrane prepared with 65% YSZ content. This work shows the feasibility to design and modulate the microstructure and properties of porous ceramic hollow fiber membranes for specific separation applications through optimizing the suspension solid content.

Acknowledgments

This work was financially supported by the National Natural Science Foundation of China (No. 51262012 and 51462012), Jiangxi Provincial Natural Science Foundation (20114BAB206022 and 20142BAB206005) and Jiangxi Provincial Fund for Excellent Young Scientists (20133BCB23019), and Jiangxi Provincial Department of Education, China (KJLD14076).

References

[1] R. Wang, B. Meng, X. Meng, X. Tan, J. Sunarso, L. Liu, S. Liu, Highly stable $La_{0.6}Sr_{0.4}Co_{0.2}Fe_{0.8}O_{3-\delta}$ hollow fibre membrane for air separation swept by steam or steam mixture, J. Membr. Sci. 479 (2015) 232–239.

[2] X. Tan, X. Tan, N. Yang, B. Meng, K. Zhang, S. Liu, High performance $BaCe_{0.8}Y_{0.2}O_{3-a}$ (BCY) hollow fibre membranes for hydrogen permeation, Ceram. Int. 40 (2014) 3131–3138.

[3] X. Tan, N. Liu, B. Meng, S. Liu, Morphology control of the perovskite hollow fibre membranes for oxygen separation using different bore fluids, J. Membr. Sci. 378 (2011) 308–318.

[4] X. Zhang, B. Lin, Y. Ling, Y. Dong, G. Meng, X. Liu, An anode-supported micro-tubular solid oxide fuel cell with redox stable composite cathode, Int. J. Hydrogen Energy 35 (2010) 8654–8662.

[5] L. Zhao, X. Zhang, B. He, B. Liu, C. Xia, Micro-tubular solid oxide fuel cells with graded anodes fabricated with a phase inversion method, J. Power Sources 196 (2011) 962–967.

[6] P. de Wit, E.J. Kappert, T. Lohaus, M. Wessling, A. Nijmeijer, N.E. Benes, Highly permeable and mechanically robust silicon carbide hollow fibre membranes, J. Membr. Sci. 475 (2015) 480–487.

[7] X. Zhang, D.K. Wang, D.R.S. Lopez, J.C.D. da Cost, Fabrication of nanostructured TiO_2 hollow fibre photocatalytic membrane and application for wastewater treatment, Chem. Eng. J. 236 (2014) 314–322.

[8] X. Zhang, B. Lin, Y. Ling, Y. Dong, D. Fang, G. Meng, X. Liu, Highly permeable porous YSZ hollow fibre membrane prepared using ethanol as external coagulant, J. Alloys Compd. 494 (2010) 366–371.

[9] S. Liu, K. Li, R. Hughes, Preparation of porous aluminium oxide (Al_2O_3) hollow fibre membranes by a combined phase inversion and sintering method, Ceram. Int. 29 (2003) 875–881.

[10] L. Liu, X. Tan, S. Liu, Yttria stabilized zirconia hollow fibre membranes, J. Am. Ceram. Soc. 89 (2006) 1156–1159.

[11] X. Zhang, D. Fang, B. Lin, Y. Dong, G. Meng, X. Liu, Asymmetric porous cordierite hollow fibre membrane for microfiltration, J. Alloys Compd. 487 (2009) 631–638.

[12] H.P. Hsieh, Inorganic Membranes for Separation and Reaction, Elsevier Science, Amsterdam, 1996.

[13] J. Zhang, H. Fang, L. Hao, X. Xu, C. Chen, Preparation of silicon nitride hollow fibre membrane for desalination, Mater. Lett. 68 (2012) 457–459.

[14] X. Zhang, J. Hu, Q. Chang, Y. Wang, J. Zhou, T. Zhao, Y. Jiang, X. Liu, Influences of internal coagulant composition on microstructure and properties of porous YSZ hollow fibre membranes for water treatment, Sep. Purif. Technol. 147 (2015) 337–345.

[15] M.A. Rahman, F.R. García-García, K. Li, Development of a catalytic hollow fibre membrane microreactor as a microreformer unit for automotive application, J. Membr. Sci. 390–391 (2012) 68–75.

[16] P. Luis, A. Garea, A. Irabien, Environmental and economic evaluation of SO_2 recovery in a ceramic hollow fibre membrane contactor, Chem. Eng. Process. 52 (2012) 151–154.

[17] K. Tao, C. Kong, L. Chen, High performance ZIF-8 molecular sieve membrane on hollow ceramic fibre via crystallizing-rubbing seed deposition, Chem. Eng. J. 220 (2013) 1–5.

[18] F.R. García-García, S.C. Tsang, K. Li, Hollow fibre based reactors for an enhanced H_2 production by methanol steam reforming, J. Membr. Sci. 455 (2014) 92–102.

[19] Y.E. Fung, H. Wang, Nickel aluminate spinel reinforced ceramic hollow fibre membrane, J. Membr. Sci. 450 (2014) 418–424.

[20] B.F.K. Kingsbury, K. Li, A morphological study of ceramic hollow fibre membranes, J. Membr. Sci. 328 (2009) 134–140.

[21] Z. Wu, R. Faiz, T. Li, B.F.K. Kingsbury, K. Li, A controlled sintering process for more permeable ceramic hollow fibre membranes, J. Membr. Sci. 446 (2013) 286–293.

[22] R.W. Field, D. Wu, J.A. Howell, B.B. Gupta, Critical flux concept for microfiltration fouling, J. Membr. Sci. 100 (1995) 259–272.

[23] N. Peng, T. Chung, K.Y. Li, The role of additives on dope rheology and membrane formation of defect-free Torlon® hollow fibres for gas separation, J. Membr. Sci. 343 (2009) 62–72.

[24] D.R. Dinger, Rheology for Ceramists, Dinger Ceramic Consulting Services, Clemson, SC, 2002.

[25] C.A. Smolders, A.J. Reuvers, R.M. Boom, I.M. Wienk, Microstructures in phase inversion membranes. Part 1. Formation of macrovoids, J. Membr. Sci. 73 (1992) 259–275.

[26] S.P. Nunes, T. Inoue, Evidence for spinodal decomposition and nucleation and growth mechanisms during membrane formation, J. Membr. Sci. 111 (1996) 93–103.

[27] C. Barth, M.C. Gonçalves, A.T.N. Pires, J. Roeder, B.A. Wolf, Asymmetric polysulfone and polyethersulfone membranes: Effects of thermodynamic conditions during formation on their performance, J. Membr. Sci. 169 (2000) 287–299.

[28] W. Li, W. Xing, N. Xu, Modeling of relationship between water permeability and microstructure parameters of ceramic membranes, Desalination 192 (2006) 340–345.
[29] M. Abbasi, A. Salahi, M. Mirfendereski, T. Mohammadi, A. Pak, Dimensional analysis of permeation flux for microfiltration of oily wastewaters using mullite ceramic membranes, Desalination 252 (2010) 113–119.
[30] Z. Zhong, W. Xing, B. Zhang, Fabrication of ceramic membranes with controllable surface roughness and their applications in oil/water separation, Ceram. Int. 39 (2013) 4355–4361.
[31] S.R.H. Abadi, M.R. Sebzari, M. Hemati, F. Rekabdar, T. Mohammadi, Ceramic membrane performance in microfiltration of oily wastewater, Desalination 265 (2011) 222–228.